An ocean coupling potential intensity index for tropical cyclones

I.-I. Lin,[1,2] P. Black,[3] J. F. Price,[4] C.-Y. Yang,[1] S. S. Chen,[5] C.-C. Lien,[1,2] P. Harr,[6] N.-H. Chi,[7] C.-C. Wu,[1] and E. A. D'Asaro[7]

Received 31 October 2012; revised 12 December 2012; accepted 13 December 2012; published 15 May 2013.

[1] Timely and accurate forecasts of tropical cyclones (TCs, i.e., hurricanes and typhoons) are of great importance for risk mitigation. Although in the past two decades there has been steady improvement in track prediction, improvement on intensity prediction is still highly challenging. Cooling of the upper ocean by TC-induced mixing is an important process that impacts TC intensity. Based on detail in situ air-deployed ocean and atmospheric measurement pairs collected during the Impact of Typhoons on the Ocean in the Pacific (ITOP) field campaign, we modify the widely used Sea Surface Temperature Potential Intensity (SST_PI) index by including information from the subsurface ocean temperature profile to form a new Ocean coupling Potential Intensity (OC_PI) index. Using OC_PI as a TC maximum intensity predictor and applied to a 14 year (1998–2011) western North Pacific TC archive, OC_PI reduces SST_PI-based overestimation of archived maximum intensity by more than 50% and increases the correlation of maximum intensity estimation from $r^2 = 0.08$ to 0.31. For slow-moving TCs that cause the greatest cooling, r^2 increases to 0.56 and the root-mean square error in maximum intensity is 11 m s^{-1}. As OC_PI can more realistically characterize the ocean contribution to TC intensity, it thus serves as an effective new index to improve estimation and prediction of TC maximum intensity.
Citation: Lin, I.-I., P. Black, J. F. Price, C.-Y. Yang, S. S. Chen, C.-C. Lien, P. Harr, N.-H. Chi, C.-C. Wu, and E. A. D'Asaro (2013), An ocean coupling potential intensity index for tropical cyclones, *Geophys. Res. Lett.*, *40*, 1878–1882, doi:10.1002/grl.50091.

1. Introduction

[2] Tropical cyclones (TCs) impose threats to a billion people each year [*Peduzzi et al.*, 2012] but current TC intensity forecasting remains a very difficult task due to the complex physical processes controlling TC intensity [*Rappaport et al.*, 2012]. Proposed in the 1980s, the Potential Intensity (PI) index is a fundamental concept and a widely used guide to estimate upper bound of TC intensity (i.e., PI) given atmospheric and ocean surface conditions [*Emanuel*, 1988, 1995, 1997; *Holland*, 1997; *Bister and Emanuel*, 1998; *Wang and Wu*, 2004; *Vecchi and Soden*, 2007]. The PI is developed based on the assumption that the TC behaves like a classic Carnot heat engine in which energy is added at the underlying warm ocean surface and lost in the cool outflow area. By incorporating eye dynamics, which is closed by assuming a balance between the radial entropy advection and the surface entropy flux together with an assumption of cyclostrophic balance, *Emanuel* [1995, 1997] showed that PI (measured by maximum surface wind) has an explicit dependence on sea surface temperature (SST), air temperature of the outflow layer in the upper troposphere, the ratio of the exchange coefficient to the drag coefficient at the air sea interface (Ck/CD), and maximum entropy difference between the cyclone center and the environment.

[3] However, as the above PI index uses only sea surface temperature (SST) to characterize the ocean contribution to cyclone intensity and does not consider the contribution from the subsurface ocean, it often grossly over-estimates (or over-predicts) the intensity upper bound [*Wang and Wu*, 2004]. Because the upper bound can be unrealistically high, when using PI as a TC maximum intensity predictor, TC peak (i.e. maximum) intensity is often grossly over-predicted. Here we modify the existing PI index and propose a revised OC (Ocean Coupling or Ocean Cooling) PI index to account for overestimation of SST_PI due to incomplete ocean information and find a substantial improvement in the performance of using PI as a predictor of TC maximum intensity.

2. Current Potential Intensity Index

[4] The energy of a TC is supplied by the warm pre-existing underlying ocean. A useful conceptual view of a TC is as a heat engine in which the warm reservoir is the ocean (characterized by *SST*), and the cold reservoir is defined as the temperature, T_0 of the outflow at the top of the TC. The PI index

$$V^2 = \frac{SST - T_0}{T_0}\frac{C_k}{C_D}(k^* - k) \tag{1}$$

predicts TC maximum intensity (in maximum surface wind speed, V), as a function of the pre-cyclone *SST* (with no cooling effect from the subsurface, hence the name SST_PI in this study), T_0 (TC outflow temperature determined by the atmospheric vertical profile), the drag coefficient, C_D, the enthalpy exchange coefficient, C_k, the saturation enthalpy of the sea surface, k^*, and the surface enthalpy in the TC environment, k. However, as a TC intensifies,

[1]Department of Atmospheric Sciences, National Taiwan University, Taipei, Taiwan.
[2]Research Center for Environmental Changes, Academia Sinica, Taipei, Taiwan.
[3]Science Application International Corporation, Inc and Naval Research Laboratory, Monterey, California, USA.
[4]Woods Hole Oceanographic Institution, Woods Hole, Massachusetts, USA.
[5]Rosenstiel School of Marine and Atmospheric Sciences, University of Miami, Miami, Florida, USA.
[6]Naval Postgraduate School, Monterey, California, USA.
[7]Applied Physics Laboratory, University of Washington, Seattle, Washington, USA.

Corresponding author: I.-I. Lin, Dept. of Atmospheric Sciences, National Taiwan University, No. 1, Sec. 4, Roosevelt Rd., Taipei 106, Taiwan. (iilin@as.ntu.edu.tw)

0094-8276/13/10.1002/grl.50091

vertical mixing and upwelling of cooler subsurface ocean water with the warm pre-cyclone surface water reduces the SST. The strength of this effect depends on the ocean subsurface thermal structure, as well as the TC translation speed, size, and wind speed [*Price*, 1981; *Emanuel*, 1999; *Bender and Ginis*, 2000; *Goni et al.*, 2009; *Lin et al.*, 2003, 2005, 2008, 2009; *Tseng et al.*, 2010; *Lin*, 2012]. Stronger cooling occurs where colder water is closer to the surface [*Price*, 1981; *Price et al.*, 1994; *Lin*, 2012]. In addition to the above-mentioned mechanical turbulent mixing and upwelling, air-sea fluxes can also contribute to SST cooling, though the effect is usually much smaller [*Price*, 1981].

3. Impacts of Typhoons on the Ocean in the Pacific (ITOP) Field Campaign

[5] ITOP was an international field experiment conducted during August to October 2010 in the western North Pacific Ocean to study the interaction between tropical cyclones and the ocean [*D'Asaro et al.*, 2011]. Atmospheric profiles were taken with dropwindsondes and oceanic profiles with Airborne EXpendable BathyThermographs (AXBTs). Both instrument systems were deployed from a U.S. WC130J aircraft. Measurements taken during the ITOP field campaign in 2010 showed the varying effects of TC-induced ocean cooling beneath three intensively measured TCs: Megi, Fanapi, and Malakas, with maximum observed winds of 82 m s^{-1} (category-5 in Saffir-Simpson scale), 54 m s^{-1} (category-3), and 46 m s^{-1} (category-2), respectively. The pre-cyclone SST of approximately 29.5°C was similar for all three cyclones (Figures 1a and 2a; see also Figure S1 and Table S1), and hence all had a similar SST_PI of approximately 75–80 m s^{-1} (category-5) (Figure 1c). Only Megi actually reached this intensity. The depth of the 26°C isotherm (D26) [*Leipper and Volgenau*, 1972; *Shay et al.*, 2000; *Lin et al.*, 2005, 2008, 2009; *Pun et al.*, 2007, 2011; *Goni et al.*, 2009] indicates the thickness of the warm ocean subsurface layer. Megi intensified over a very thick warm layer with D26 ~110 m. Fanapi and Malakas intensified in regions with thinner warm layers (i.e., colder subsurface water is closer to the surface), with D26 near 70 and 45 m, respectively (Figure 2a).

[6] Co-located profiles of atmospheric and oceanic properties obtained from aircraft deployments (locations depicted in Figure 1b), combined with pre-cyclone ocean temperature profiles from operational ARGO floats [*Gould et al.*, 2004], measured ocean cooling beneath each cyclone (Figure 2b). Fanapi and Malakas induced much more SST cooling than Megi. Throughout the intensification of Megi, the SST beneath the cyclone remained at ~29°C (Figure 2b, blue triangles with error bars). The air-sea temperature and humidity differences remained nearly constant (Figures S8A and S8B), hence the air-sea enthalpy (latent plus sensible heat) fluxes increased with increasing wind speed (Figure 2c, blue triangles with error bars). In contrast, the SST beneath Fanapi and Malakas was cooler at approximately 27–28°C (Figure 2b, black and red triangles with error bars), and the air-sea temperature and humidity differences decreased with increasing wind speed (Figures S8A and S8B). The resulting air-sea fluxes increased with wind speed up to approximately

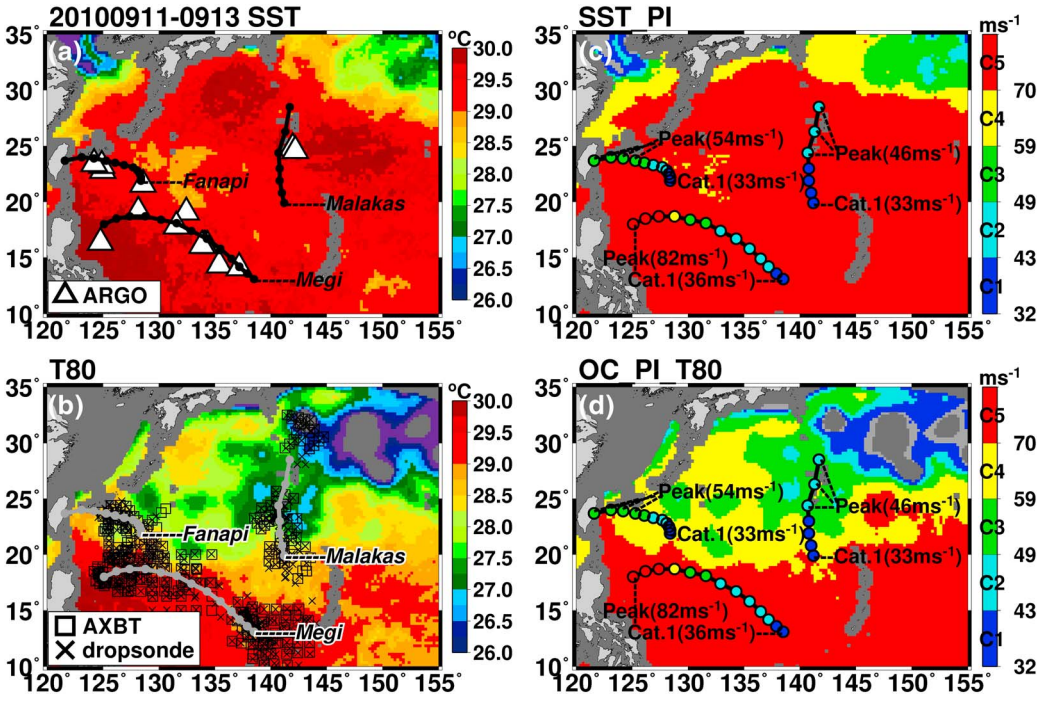

Figure 1. (a) Pre-cyclone SST (color) at the start (11–13 September 2010) of the ITOP field campaign. Intensification tracks (from first point in category-1 to peak) of the three ITOP TCs are shown by black circles. White triangles show locations of nearby, pre-cyclone, Argo float temperature profiles. (b) As in Figure 1a, but for pre-cyclone T80 (temperature averaged over top 80 m) computed from satellite altimetry. Symbols show locations of the dropwindsonde and AXBT profiles. (c) SST_PI (computed using SST from Figure 1a) indicated by color (C1–C5 indicates intensity categories). Intensification tracks and intensities of the three ITOP cases are shown by colored circles. (d) As in Figure 1c but OC_PI_T80 using T80 from Figure 1b.

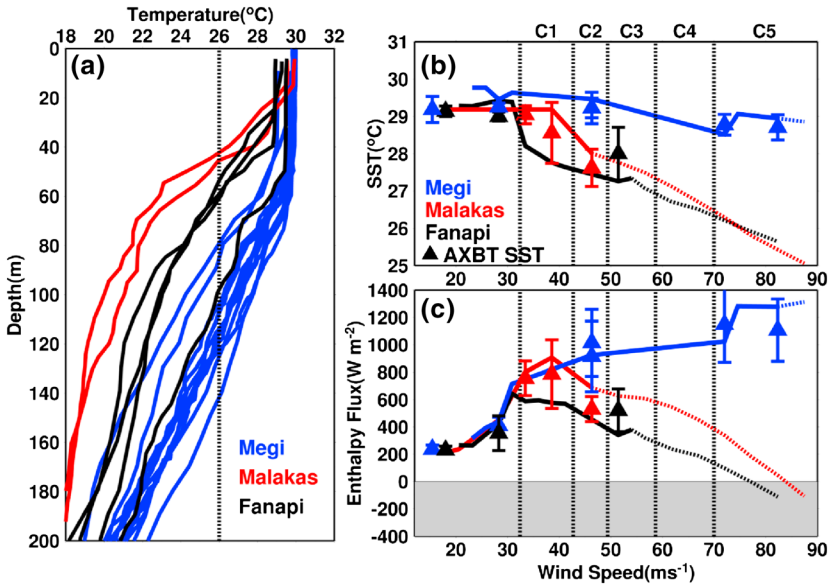

Figure 2. (a) Pre-cyclone ocean temperature profiles from ARGO floats color-coded by TC cases. (b) During intensification mean SST (triangles) with standard deviation (error bars) from AXBTs within 34 kt wind radius of each cyclone. Simulation of SST evolution for each cyclone during intensification (solid lines) with additional simulations with wind speeds up to 90 m s^{-1} (dashed lines). (c) As in Figure 2b, but for the corresponding air-sea enthalpy flux supply during intensification (see also auxiliary material).

35 m s^{-1}, but decreased at higher wind speeds (Figure 2c). We hypothesize that this reduction in enthalpy fluxes caused by SST cooling was a key factor preventing Fanapi and Malakas from intensifying to the full strength predicted by their SST_PI.

[7] Simulations of ocean cooling using a 3D ocean mixed layer model [*Price et al.*, 1994] predict the observed changes in SST for all three cyclones to within the measurement error (Figure 2b, solid lines). We test the hypothesis by conducting additional simulations with wind speeds up to 90 m s^{-1} (Figure 2b, dashed lines). With increasing winds, the ocean cooling increases and the air-sea enthalpy flux decreases for Fanapi and Malakas (Figure 2c) to reach zero near 80 m s^{-1}. In contrast, the fluxes were greater for Megi throughout its intensification (Figure 2c). Because the ocean is the energy source for intensification [*Bister and Emanuel*, 1998; *Emanuel*, 1999], these nearly zero fluxes could not have supported intensification of Fanapi and Malakas to their SST_PI, even if the atmospheric conditions were favourable.

4. The New Ocean Coupling (or Ocean Cooling) Potential Intensity Index

[8] A new index, OC_PI, is proposed to include the effect of ocean cooling by substituting the pre-cyclone depth-averaged (averaged from the surface down to the expected cyclone-induced mixing depth) ocean temperature, $\bar{T}$, for a pre-cyclone *SST*:

$$V_{OC\_PI}{}^2 = \frac{\bar{T} - T_0}{T_0}\frac{C_k}{C_D}(k^* - k) \tag{2}$$

[9] This is because the pre-cyclone depth-averaged $\bar{T}$ is a good approximation of the sea surface temperature during the TC intensification (i.e., the SST affected by subsurface mixing) [*Price*, 2009]. Although the mixing depth depends on the TC translation speed, size, and intensity, and on the upper ocean thermal structure [*Price*, 1981; *Price et al.*, 1994; *Lin et al.*, 2003, 2005, 2008, 2009; *Price*, 2009], it is typically 60–100 m [*Price*, 2009]. A series of OC_PI for $\bar{T}$ from T20 to T100 (i.e., 20–100 m mixing depth) thus was computed for analysis (Figures 3, 4, and S9). Here in Figures 1 and 3, we illustrate the results using T80 (denoted as OC_PI_T80) because it was found to be a convenient first-guess choice to illustrate the concept of OC_PI (see detail discussions for depth choices in the auxiliary material). Figures 1b and 1d show pre-ITOP $\bar{T}$ (for T80) and the predicted OC_PI_T80. For Megi, $\bar{T}$ is close to the sea surface temperature (Figures 1a and 1b) and the OC_PI_T80 is close to the SST_PI (Figures 1c and 1d). Both indices predict maximum (peak) intensity well. For Fanapi and Malakas, the maximum intensity predicted by OC_PI_T80 are 64 and 57 m s^{-1}, respectively, much closer to their actual maximum intensities than the SST_PI (75–80 m s^{-1}) (Figures 1c and 1d). Besides the above fixed-depth approach, a more precise mixing depth and $\bar{T}$ may also be obtained by using the cyclone translation speed, wind speed, and pre-cyclone upper ocean thermal profile as inputs to the *Price* [2009] estimation model (program available from http://www.whoi.edu/jpweb/Td.f). Examples based on translation speeds of 3 and 6 m s^{-1} and the associated OC_PI for the case of Fanapi are shown in Figure S10. It can be seen that a slower translation speed (i.e. 3 m s^{-1}, $\bar{T}$ is smaller and resulted in smaller OC_PI).

[10] A statistical comparison of OC_PI and SST_PI was made using 1998–2011 best-track estimates of cyclone track and intensity from the U.S. Joint Typhoon Warning Center. All cases during western North Pacific TC season (July–October) between 1998 and 2011 were

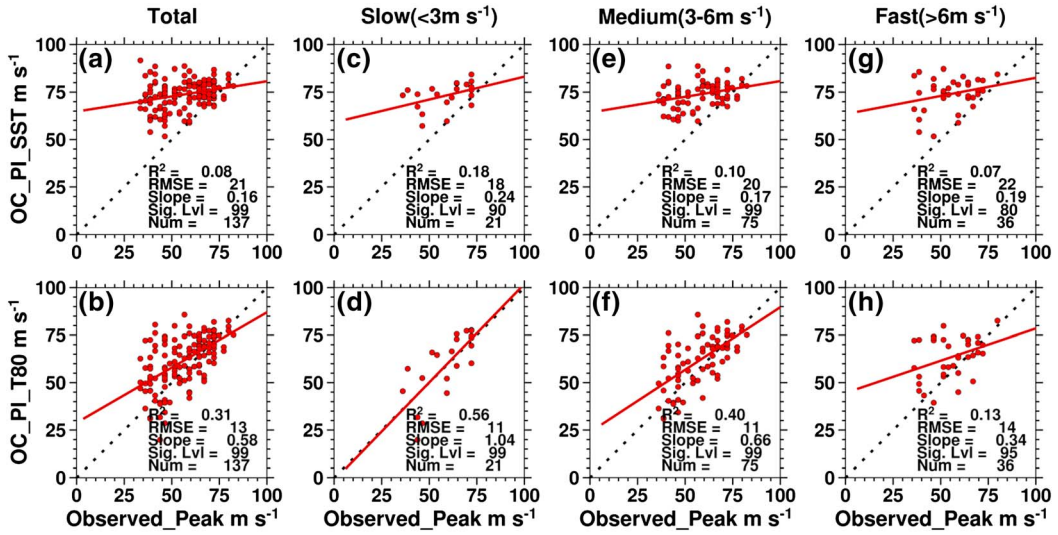

Figure 3. Scatter plots of observed maximum TC intensity from SST_PI (top row, a, c, e, and g) and OC_PI (bottom row, b, d, f, and h). Columns subdivide the data by TC translation speed.

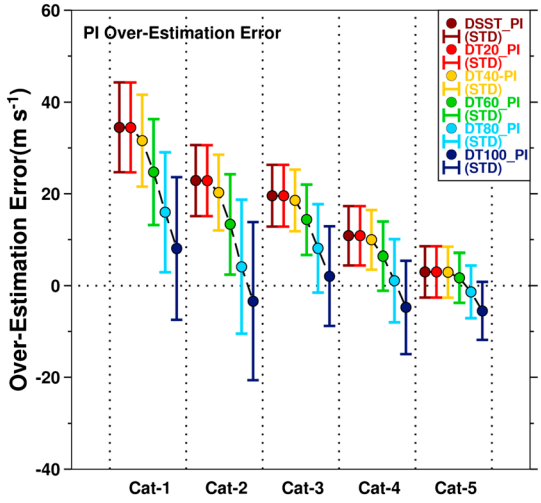

Figure 4. The TC maximum intensity estimation error for SST_PI (brown) and OC_PI for various depths of temperature profile averaging (see legend).

examined. Average values of SST_PI and OC_PI were computed along the track locations from category-1 to peak. Inputs were based on pre-cyclone (2 days before category-1) atmospheric (reanalysis data from the European Centre for Medium Range Weather Forecasts) and ocean information. Ocean inputs (i.e., SST and $\bar{T}$) were calculated from pre-cyclone temperature profiles estimated from satellite SST and altimetry [*Shay et al.*, 2000; *Pun et al.*, 2007; *Goni et al.*, 2009] (for details see auxiliary material).

[11] The SST_PI has little correlation ($R^2 = 0.08$, slope = 0.16) with the observed maximum intensity (Figure 3a). OC_PI has a higher correlation, with $R^2 = 0.31$ and a slope of 0.58 for OC_PI_T80 (Figure 3b). The OC_PI_T80 also greatly reduces the overestimation of TC maximum intensity by SST_PI (Figure 4), from 34 to 15 m s^{-1} (56%) for category-1 TCs and from 19 to 8 m s^{-1} (58%) for category-3 TCs (Figure 4). Greater skill for OC_PI_T80 is achieved by segregating TCs by translation speed. Estimation of PI for slow TCs (0–3 m s^{-1}), which exhibit the greatest ocean cooling [*Price*, 1981; *Price et al.*, 1994; *Lin et al.*, 2009], exhibits the greatest improvement with $R^2 = 0.56$, a slope of 1.04, and a root mean square (RMS) error of only 11 m s^{-1} (Figure 3d). For moderate and fast TCs, OC_PI_T80 also has higher correlations than SST_PI (Figures 3e–3h). The above results show that through inclusion of more complete ocean information, it is possible to improve prediction and estimation of TC intensity upper bound, hence improvement in TC maximum intensity prediction can be achieved. However, it should be cautious in the determination of the mixing depth to avoid over-use of the subsurface information (i.e. over-cooling). As illustrated in Figure 4, the choice of 100m mixing depth (i.e. T100) can lead to over-cooling of certain cases and under-predict the intensity upper bound and maximum intensity.

5. Discussion and Conclusion

[12] With the advent of global ARGO floats and ocean depth-temperature profile estimation by means of satellite altimetry [*Shay et al.*, 2000; *Pun et al.*, 2007, 2011; *Goni et al.*, 2009], it is now possible to operationally incorporate subsurface ocean information into quasi-dynamical TC intensity estimates, such as OC_PI. We have shown that this approach improves hindcasts of TC maximum intensity and anticipate that similar approaches would contribute to improvements in forecasts. For instance, currently the best-performing intensity-prediction model is the U.S. National Oceanic and Atmospheric Association (NOAA)'s statistical model [*DeMaria et al.*, 2005; *Mainelli et al.*, 2008], in which SST_PI is used as a key predictor. It would be interesting to explore replacing SST_PI with OC_PI as OC_PI can more realistically characterize the ocean contribution to TC maximum intensity. For physical-based predictions, it also provides a baseline for new generation of fully coupled atmosphere-wave-ocean models [*Chen et al.*, 2007].

[13] The TC-induced ocean cooling is one of the factors controlling tropical cyclone intensity [*Wang and Wu*, 2004; *DeMaria et al*., 2005; *Houze et al*., 2007]. Atmospheric wind shear and TC internal dynamics such as eyewall replacement cycles are also influential [*Frank and Ritchie*, 2001; *DeMaria et al*., 2005; *Houze et al*., 2007; Tang and Emanuel, in press). Our analysis suggests that these non-ocean factors should be relatively more (less) important for fast (slow)-moving TCs, where the OC_PI shows the smallest (largest) improvement (Figures 3g, 3h, and S9). Very likely, atmospheric-based approaches, for example the recently proposed ventilation index (an improved characterization of the shear impact) [Tang and Emanuel, in press]) may be more effective for these TCs. Ultimately, a combined approach based on improved new approaches from both atmosphere (e.g., ventilation index) and ocean (e.g., OC_PI) may yield the best results for intensity estimation and prediction improvement.

[14] Finally, it could be helpful to use OC_PI to explore further in the context of climate change. Instead of considering only the change in SST [*Vecchi and Soden*, 2007], change in subsurface ocean thermal condition (for example, recent rapid warming in the western North Pacific Ocean [*Pun et al*., 2013]) can also be included in projecting future TC activities.

[15] **Acknowledgments.** This work is supported by Taiwan's National Science Council and National Taiwan University (grant numbers: NSC 101-2111-M-002-002-MY2; NSC 101-2628-M-002-001-MY4; 102R7803) and US Office of Naval Research (ONR) under the Impact of Typhoons on Pacific (ITOP) program. Many thanks to Kerry Emanuel for providing the SST_PI program, to David Tang for leading the Taiwan ITOP component, to NASA, AVISO, Argo, RSS for essential data sets, to the U.S. Air Force for executing the airborne data collection, and to the Reviewers for very helpful and constructive comments. PB's support is provided by ONR under PE 0601153N through NRL Contract N00173-10-C-6019.

References

Bender, M. A., and I. Ginis (2000), Real case simulation of hurricane-ocean interaction using a high-resolution coupled model: Effects on hurricane intensity, *Mon. Weather Rev.*, *128*, 917–946.

Bister, M., and K. A. Emanuel (1998), Dissipative heating and hurricane intensity, *Meteor. Atmos. Phys.*, *52*, 233–240.

Chen, S. S., J. F. Price, W. Zhao, M. A. Donelan, and E. J. Walsh (2007), The CBLAST-Hurricane Program and the next-generation fully coupled atmosphere-wave-ocean models for hurricane research and prediction, *Bull. Am. Meteor. Soc.*, *88*, 311–317.

D'Asaro, E. A., et al. (2011), Typhoon-ocean interaction in the western North Pacific, part 1. *Oceanography*, *24*, 24–31.

DeMaria, M., M. Mainelli, L. K. Shay, J. A. Knaff, and J. Kaplan (2005), Further improvements to the Statistical Hurricane Intensity Prediction Scheme (SHIPS), *Weather Forecast.*, *20*, 531–543.

Emanuel, K. A. (1988), The maximum intensity of hurricanes, *J. Atmos. Sci.*, *45*, 1143–1155.

Emanuel, K. A. (1995), Sensitivity of tropical cyclones to surface exchange coefficients and a revised steady-state model incorporating eye dynamics, *J. Atmos. Sci.*, *52*, 3969–3976.

Emanuel, K. A. (1997), Some aspects of hurricane inner-core dynamics and energetics, *J. Atmos. Sci.*, *54*, 1014–1026.

Emanuel, K. A. (1999), Thermodynamic control of hurricane intensity, *Nature*, *401*, 665–669.

Frank, W. M., and E. A. Ritchie (2001), Effects of vertical wind shear on the intensity and structure of numerically simulated hurricanes, *Mon. Weather Rev.*, *129*, 2249–2269.

Goni, G., et al. (2009), Application of satellite-derived ocean measurements to tropical cyclone intensity forecasting, *Oceanography*, *22*(3), 190–197.

Gould, J., et al. (2004), Argo profiling floats bring new era of in situ ocean observations, *EOS, Trans. Am. Geophys. Union*, *85*, 190–191.

Holland, G. J. (1997), The maximum potential intensity of tropical cyclones, *J. Atmos. Sci.*, *54*, 2519–2541.

Houze, R. A. Jr., S. S. Chen, B. F. Smull, W. C. Lee, and M. M. Bell (2007), Hurricane intensity and eyewall replacement, *Science*, *315*, 1235–1239.

Leipper, D. F., and D. Volgenau (1972), Hurricane heat potential of the Gulf of Mexico, *J. Phys. Oceanogr.*, *2*, 218–224.

Lin, I. I., W. T. Liu, C. C. Wu, G. T. F. Wong, C. Hu, Z. Chen, W. D. Liang, Y. Yang, and K. K. Liu (2003), New evidence for enhanced ocean primary production triggered by tropical cyclone, *Geophys. Res. Lett.*, *30*(1718), doi:10.1029/2003GL017141.

Lin, I. I., C. C. Wu, K. A. Emanuel, I. H. Lee, C. R. Wu, and I. F. Pun (2005), The Interaction of Supertyphoon Maemi (2003) With a Warm Ocean Eddy, *Mon. Wea. Rev.*, *133*, 2635–2649.

Lin, I. I., C. C. Wu, I. F. Pun, and D. S. Ko (2008), Upper-Ocean Thermal Structure and the Western North Pacific Category-5 Typhoons. Part I: Ocean Features and Category-5 Typhoon's Intensification, *Mon. Wea. Rev.*, *136*, 3288–3306, doi:10.1175/2008MWR2277.1.

Lin, I. I., I. F. Pun, and C. C. Wu (2009), Upper ocean thermal structure and the western North Pacific category-5 typhoons—Part II: Dependence on translation speed, *Mon. Weather Rev.*, *137*, 3744–3757.

Lin, I. I. (2012), Typhoon-induced phytoplankton blooms and primary productivity increase in the western North Pacific Subtropical Ocean, *J. Geophys. Res.*, *117*, C03039, doi:10.1029/2011JC007626.

Mainelli, M., M. DeMaria, L. K. Shay, and G. Goni (2008), Application of oceanic heat content estimation to operational forecasting of recent Atlantic category 5 hurricanes, *Weather Forecast.*, *23*, 3–16.

Peduzzi, P., et al. (2012), Global trends in tropical cyclone risk, *Nature Clim. Change*, *2*, 289–294.

Price, J. F. (1981), Upper ocean response to a hurricane, *J. Phys. Oceanogr.*, *11*, 153–175.

Price, J. F., T. B. Sanford, and G. Z. Forristall (1994), Forced stage response to a moving hurricane, *J. Phys. Oceanogr.*, *24*, 233–260.

Price, J. F. (2009), Metrics of hurricane-ocean interaction: Vertically-integrated or vertically-averaged ocean temperature? *Ocean Sci.*, *5*, 351–368.

Pun, I. F., I. I. Lin, C. R. Wu, D. S. Ko, and W. T. Liu (2007), Validation and application of altimetry-derived upper ocean thermal structure in the western North Pacific ocean for typhoon intensity forecast, *IEEE Trans. Geosci. Remote Sens.*, *45*, 1616–1630.

Pun, I. F., Y. T. Chang, I. I. Lin, T. Y. Tang, and R. C. Lien (2011), Typhoon-Ocean Interaction in the Western North Pacific, Part 2, *Oceanography*, *24*(4), 32–41, doi:10.5670/oceanog.2011.92.

Pun, I. F., I. I. Lin, and M. H. Lo (2013), Recent increase in high tropical cyclone heat potential area in the western North Pacific Ocean, *Geophys. Res. Lett.*, doi:10.1002/grl.50548.

Rappaport, E. N., J. G. Jiing, C. W. Landsea, S. T. Murillo, and J. L. Franklin (2012), The joint hurricane testbed—Its first decade of tropical cyclone research-to-operations activities revisited, *Bull. Am. Meteor. Soc.*, *93*, 371–380.

Shay, L. K., G. J. Goni, and P. G. Black (2000), Role of a warm ocean feature on Hurricane Opal, *Mon. Weather Rev.*, *128*, 1366–1383.

Tang, B., and K. Emanuel, (in press), A ventilation index for tropical cyclones, *Bull. Am. Meteor. Soc.*

Tseng, Y.-H., S. Jan, D. E. Dietrich, I. I. Lin, Y. T. Chang, and T. Y. Tang (2010), Modeled Oceanic Response and sea surface cooling to Typhoon Kai-Tak, *Terr. Atmos. Ocean. Sci.*, *21*(1), 85–98, doi:10.3319/TAO.2009.06.08.02(IWNOP).

Vecchi, G. A., and B. J. Soden (2007), Effect of remote sea surface temperature change on tropical cyclone potential intensity, *Nature*, *450*, 1066–1070.

Wang, Y., and C. C. Wu (2004), Current understanding of tropical cyclone structure and intensity changes—A review, *Meteor. Atmos. Phys.*, *87*, 257–278.

Supporting Online Material for:

An Ocean Cooling Potential Intensity Index for Tropical Cyclones

(by Lin et al.)

Materials, Methods, and Additional Points:

1. Satellite Sea Surface Temperature (SST) data: daily, 0.25° observational composite from NASA's Tropical Rainfall Measuring Mission (TRMM) Microwave Imager (TMI) and AMSR-E (Advanced Microwave Scanning Radiometer) satellite sensors. Data source: Remote Sensing Systems (RSS).

2. *In situ* during-cyclone SST, near ocean surface atmospheric temperature (T_a) and humidity (q_a) data: during ITOP field campaign, three TC cases (Fanapi, Malakas, and Megi) were intensively observed before, during, and after TC's passing. More than 600 pairs of near co-incident and co-located profiles of atmospheric and oceanic properties were obtained using a combination of dropwindsonde and AXBT (Airborne Expendable BathyThermographs) probes deployed from a WC-130J aircraft of the United States Air Force 53rd Weather Reconnaissance Squadron (Hurricane Hunters). This work focus on data acquired during the intensification period. During subsequent intensification periods of each case, multiple TC-penetrating flights with observational focus on cyclone's inner core air-sea environment, were conducted. There were 4 flights for Fanapi, 3 flights for Malakas, and 6 flights for Megi (Fig. S7).

3. Altimetry-derived upper ocean temperature profiles and depth-averaged ocean temperature ($\overline{T}$, i.e., T20-T100) series: based on satellite derived pre-cyclone upper ocean thermal profile, $\overline{T}$ can be calculated as an average from surface down to different depths. For each of the 0.25° by 0.25° grid in the western North Pacific ocean (domain: 110-170°E, 10-30°N), pre-cyclone (2 days before category-1 intensity) upper ocean thermal profiles were first estimated for each case. The SST component of the profile was taken from the daily TRMM/TMI and AMSR-E observations (see Sec.1). The subsurface components, i.e., the depth of the 20°C and 26°C isotherms (D20 and D26), were derived using the corresponding pre-cyclone satellite altimetry Sea Surface Height Anomaly (SSHA) observations. SSHA data was used as input to a two-layer reduced gravity ocean model proposed by Shay *et al.* (2000). A simple schematic illustration is given below (after Pun *et al.* 2007). The applicability and accuracy of this satellite-derived subsurface information over the western North Pacific ocean has been validated using more than 5000 *in situ* Argo float profiles. The pre-cyclone SSHA data was based on the along-track SSHA data from multiple satellite altimetry missions, including TOPEX/Poseidon, Jason-1, Jason-2, ERS-1, ERS-2, and ENVISAT altimeters. These along-track data was gridded to 0.25° by 0.25° at every 10-day altimetry cycle prior to cyclone's passing. Data source: daily, delayed-mode along track data from the AVISO (Archiving, Validation and Interpretation of Satellite Oceanographic Data) data base (http://www.aviso.oceanobs.com/). As microwave-based SST data is available only from 1998, the $\overline{T}$ series were derived for the 1998 to 2011 TC cases.

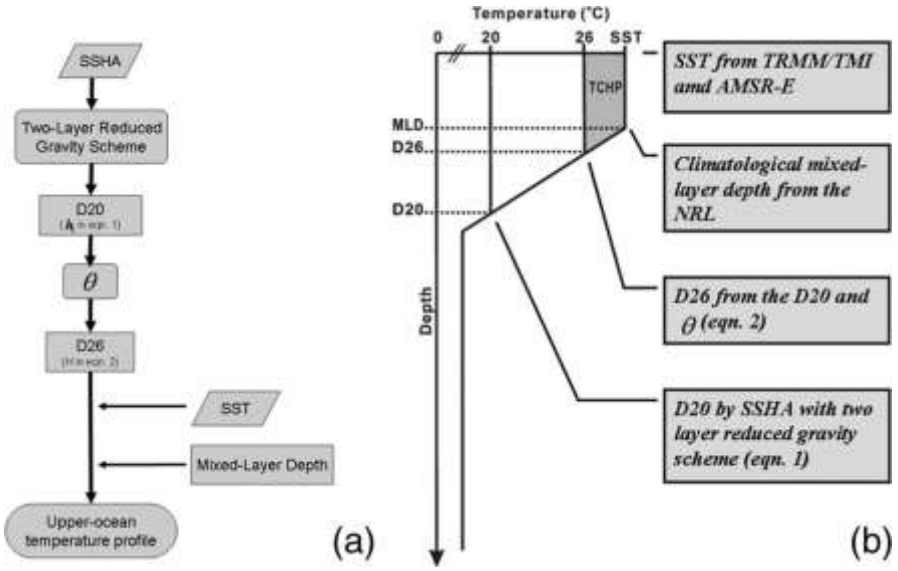

4. Air-sea enthalpy (sensible + latent heat) flux calculation: during-intensification air-sea Sensible Heat Flux (SHF) and Latent Heat Flux (LHF) calculation was based on the bulk aerodynamic formula as follows:

$$SHF:\ Q_S = C_H W\ \ T_s - T_a\ \ \rho_a C_{pa}$$

$$LHF:\ Q_L = C_E W\ \ q_s - q_a\ \ \rho_a L_{va}$$

where C_H and C_E are the sensible and latent heat exchange coefficients (Black *et al.* , *Bull. Am. Meteorol. Soc.* **88**, 357-374 (2007)), W is the wind speed, T_S and T_a are SST and near surface air temperature, q_s and q_a are surface and air specific humidity, ρ_a , C_{pa} , and L_{va} are air density, heat capacity of the air, and latent heat of vaporization. The during-intensification SST, near surface atmospheric temperature and humidity data was based on the *in situ* AXBT and dropwindsonde observations (see Sec. 2). The results are presented in Figs. 2C and S8 (points with error bars). The solid and dash lines in Figs. 2C and S8 were based on the simulated during-TC SST from the 3D ocean mixed layer simulations (Price et al. 1994,*Sec. 5*).

5. Three-dimensional ocean modeling

During-TC SST was simulated for each of the 3 ITOP cases (solid and dashed lines in Fig. 2B) for further diagnosis of the air-sea heat fluxes, and to complement *in situ* observations. The ocean model was the 3DPWP model of Price et al. (1994). This model solves for the wind-driven, baroclinic ocean response, including a treatment of turbulent vertical mixing in the upper ocean. The horizontal resolution was 5 km and the vertical resolution was 5 m. Simulations were performed for the periods of intensification, from the 1st time of TC strength to peak strength. The initial ocean temperature profiles were based on the nearest *in situ* pre-cyclone (within 1 week prior to TC's passing) upper ocean temperature profiles acquired by Argo floats at locations within 0.5 degree along TC tracks. The 2D wind field input was calculated based on the corresponding US Joint Typhoon Warning Center (JTWC)'s Best Track maximum intensity and radius of maximum wind information.

6. Potential Intensity (PI) calculation: SST_PI was calculated based on Emanuel's PI program. Eqn. A is a simple form describing the basic concept (Emanuel 1988; 1995; 1997; Bister and Emanuel 1998), the actual algorithms used is based on Bister and Emanuel (*J. Geophy. Res.*, **107**, 4801 (2002)), as below:

$$V_m^{\,2} = \frac{T_s}{T_0}\frac{C_k}{C_D}\left[CAPE^* - CAPE \right]\Big|_m \,,\; c_p T_s \ln\frac{p_0}{p_m} = \frac{1}{2}V_m^{\,2} + CAPE\Big|_m$$

$CAPE^*$ is the convective available potential energy of air lifted from saturation at sea level in reference to the environmental sounding, $CAPE$ is that of boundary layer air (not saturated), c_p is the specific heat capacity at constant pressure, p_0 is the ambient surface pressure, and p_m is the surface pressure at the RMW (Radius of the Maximum Wind). The SST input was from the pre-cyclone satellite TRMM/TMI and AMSR-E observations (Sec. 1). The atmospheric input was based on the pre-cyclone daily atmospheric temperature and humidity profile data of ECMWF (European Centre for Medium-Range Weather Forecasts)'s Interim Reanalysis database at each 1.5 degree grid over the western North Pacific Ocean. Based on the atmospheric profile input and SST, $CAPE^*$ and $CAPE$ can be calculated. In this research, PI index is used as a predictor for hindcasting maximum intensity, thus pre-cyclone (2 days before TC strength) atmospheric and ocean inputs were used. T_0, as estimated by the pre-cyclone atmospheric profile, therefore represents the tropopause temperature and was used as a proxy for TC outflow layer temperature. Default setting of the original programme for C_k / C_D was used. As the focus of this study is on ocean's impact, for OC_PI calculations, except replacing SST with series of $\overline{T}$ (i.e., T20 to T100, Sec. 3), all the other inputs were identical to SST_PI calculation.

7. Choice of $\overline{T}$: T80 is a simple and convenient choice, since mixing depth is typically in the range of 60-100m (Price 2009). As seen in Figs. 3, 4 and S9, the choice of T80 leads to significant improvement in all categories of TCs. On the other hand, the original (illustrative) choice T100 (Price 2009) overestimates most cooling events, and gives less effective hindcasts (i.e., slope > 1, see Fig. S9J). If a more precise mixing depth is required, then the cyclone's translation speed, wind speed, and pre-cyclone upper ocean thermal profile can be used as inputs to Price's $\overline{T}$ estimation model (Price 2009). Examples based on translation speeds of 3 and 6 m s^{-1} for the case of Fanapi are shown in Fig. S10. It can be seen that as Fanapi was relatively-slow moving (average translation speed = 3.2 m s^{-1}), OC_PI based on 3 m s^{-1} was close to the observed peak, while OC_PI based on 6 m s^{-1} (less cooling) does not perform as well because of over-estimation.

8. Further discussion on Potential Intensity (PI) calculation: In Eqn. B, $\overline{T}$ is used to replace SST in Eqn. A and the rest of the equation remains the same. This indicates that the atmospheric part, like CAPE*-CAPE (section 6) is the same. This is under the assumption that the air profile does not have sufficient time to adjust to the new SST so quickly. If more time is allowed for the air profile to adjust to the new SST through replacing the lowest level air temperature with $\overline{T}$ and re-do the OC_PI calculation, there is a further reduction in OC_PI by about 10-20%. As seen in Fig. S11, the new OC_PI (Fig. S11d) is lower than the existing OC_PI (Fig. S11b) by about 5-15 m s^{-1} (Fig. S11c). It is also much lower than the original SST_PI (Fig. S11a).

Supplementary Figures:

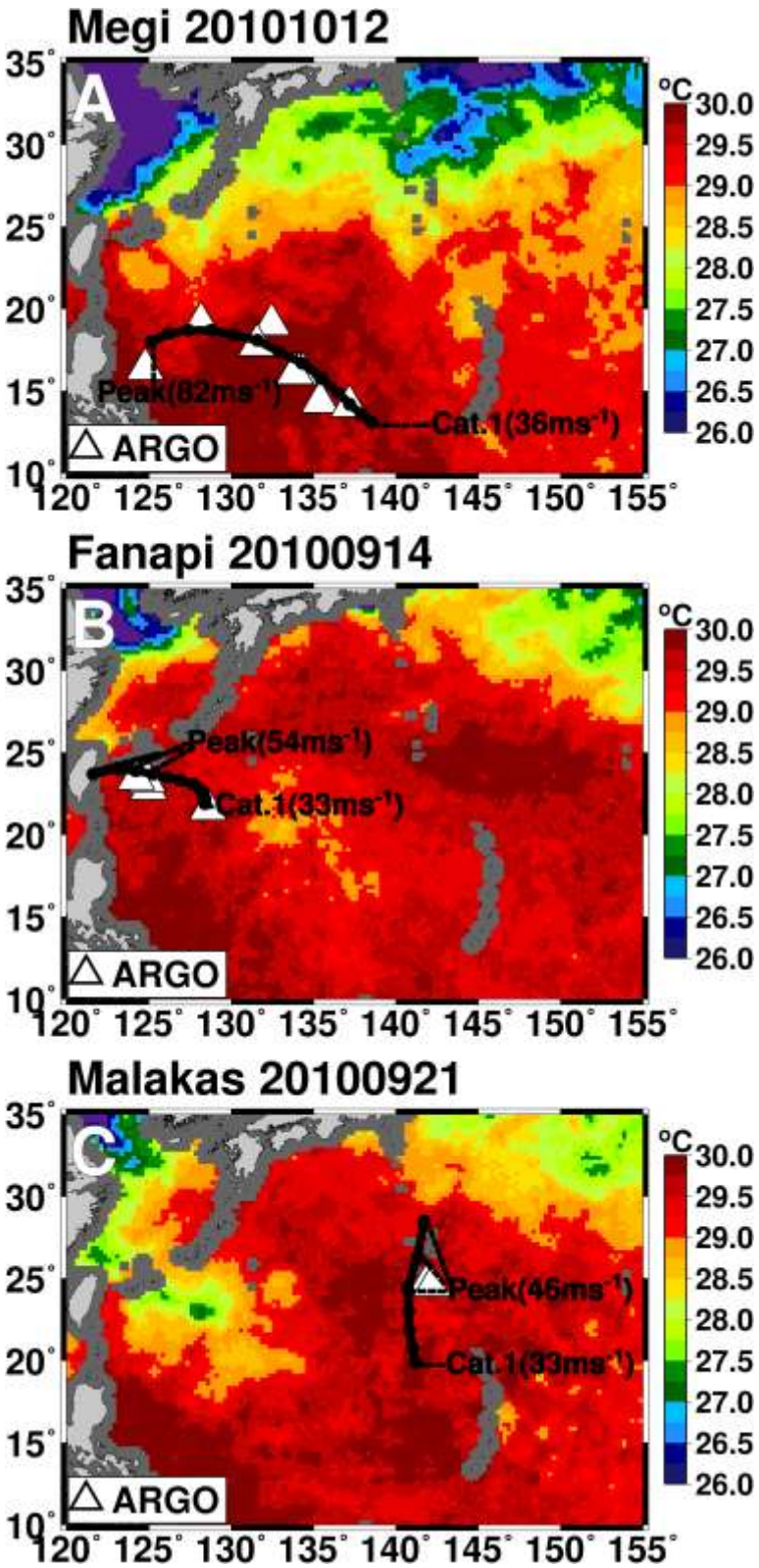

Fig. S1: Pre-cyclone (2-days before observation of category-1) SST conditions observed by the TRMM and AMSR-E satellites for the three ITOP cases. Order from top: Megi, Fanapi, and Malakas.

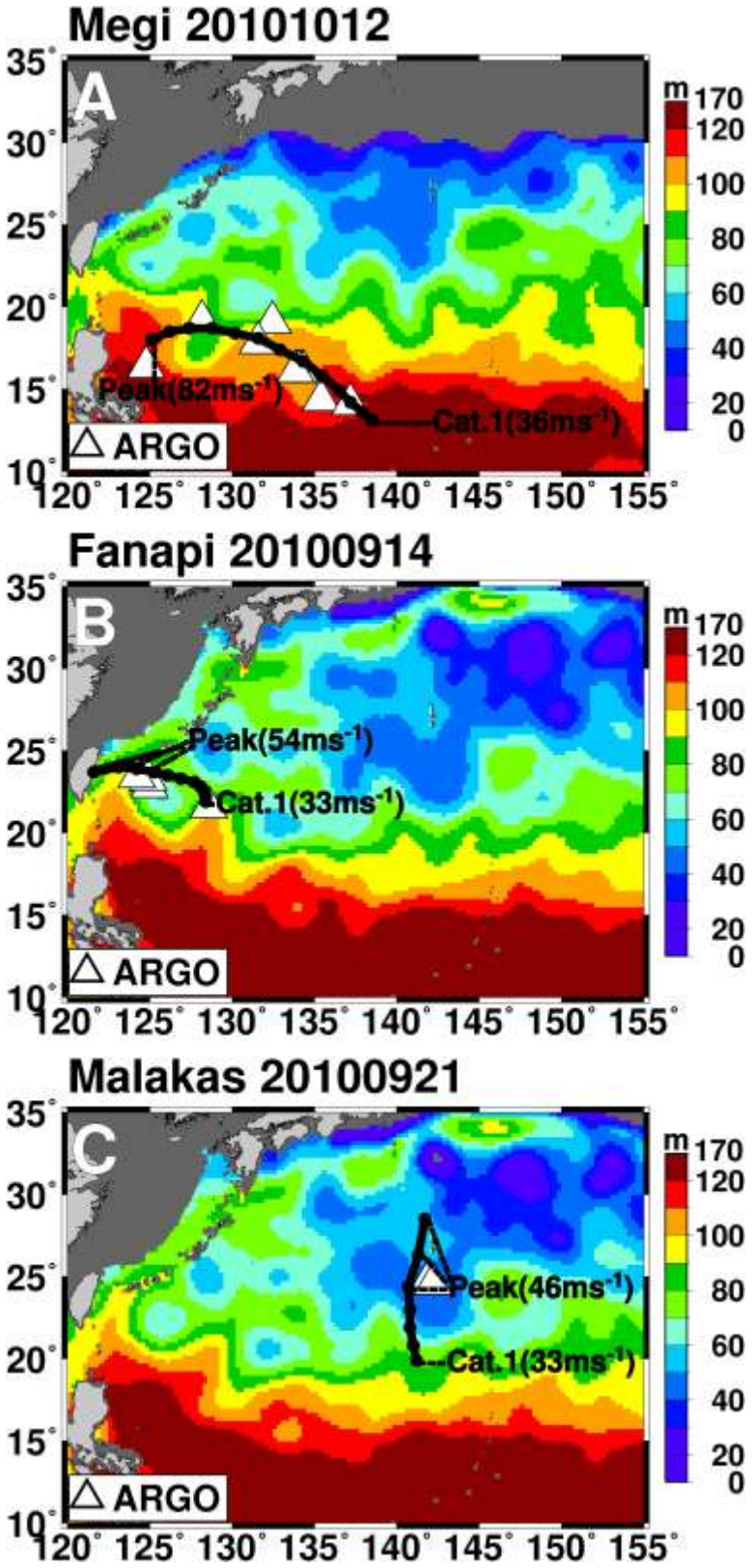

Fig. S2: As in S1, but for the corresponding pre-cyclone subsurface condition in D26.

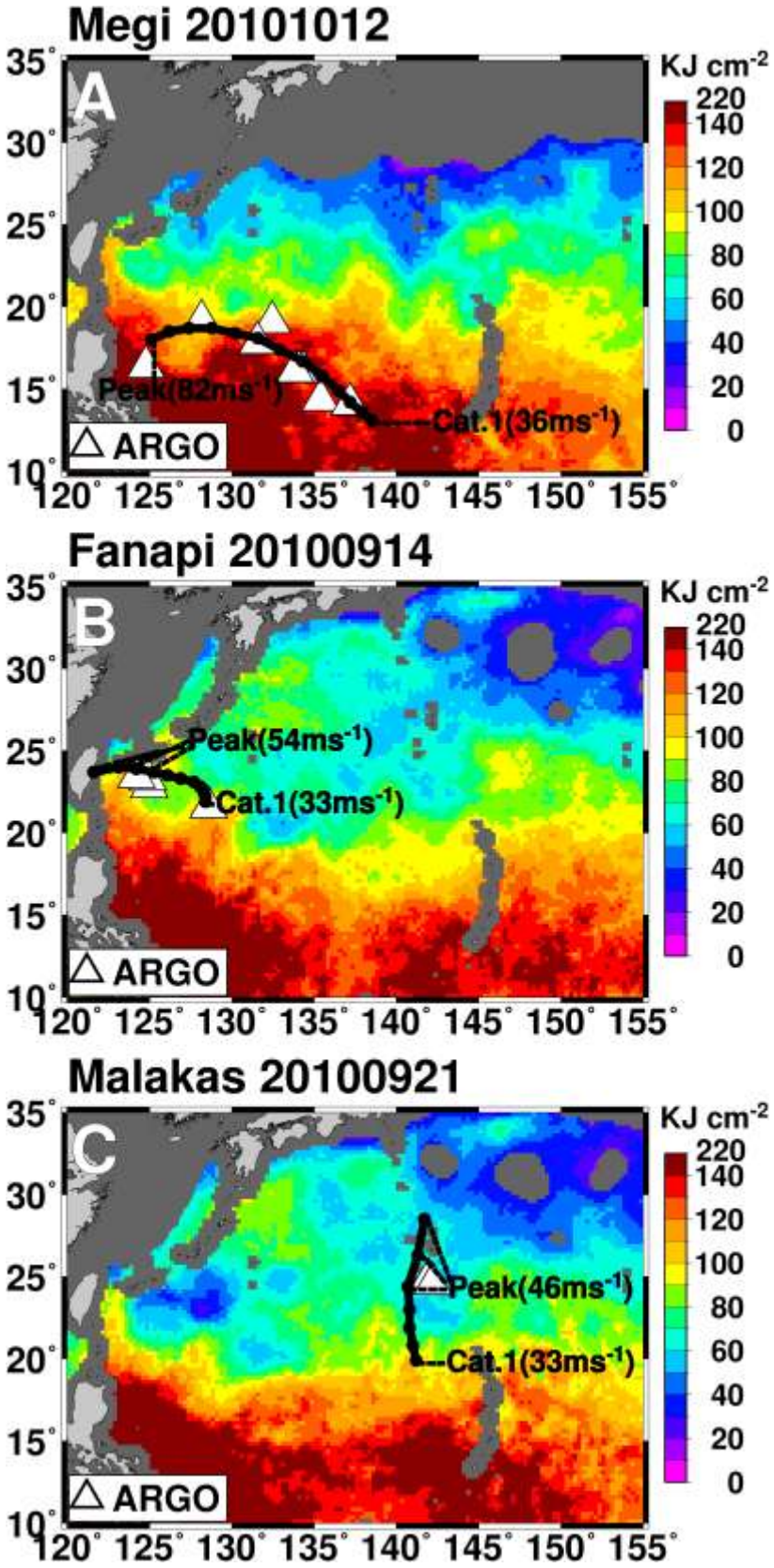

Fig. S3: As in S2, but for the corresponding pre-cyclone subsurface condition in Upper Ocean Heat Content (UOHC, i.e., depth-integrated heat content from ocean surface down to D26 (Shay et al. 2000; Pun et al. 2007; Goni et al. 2009)).

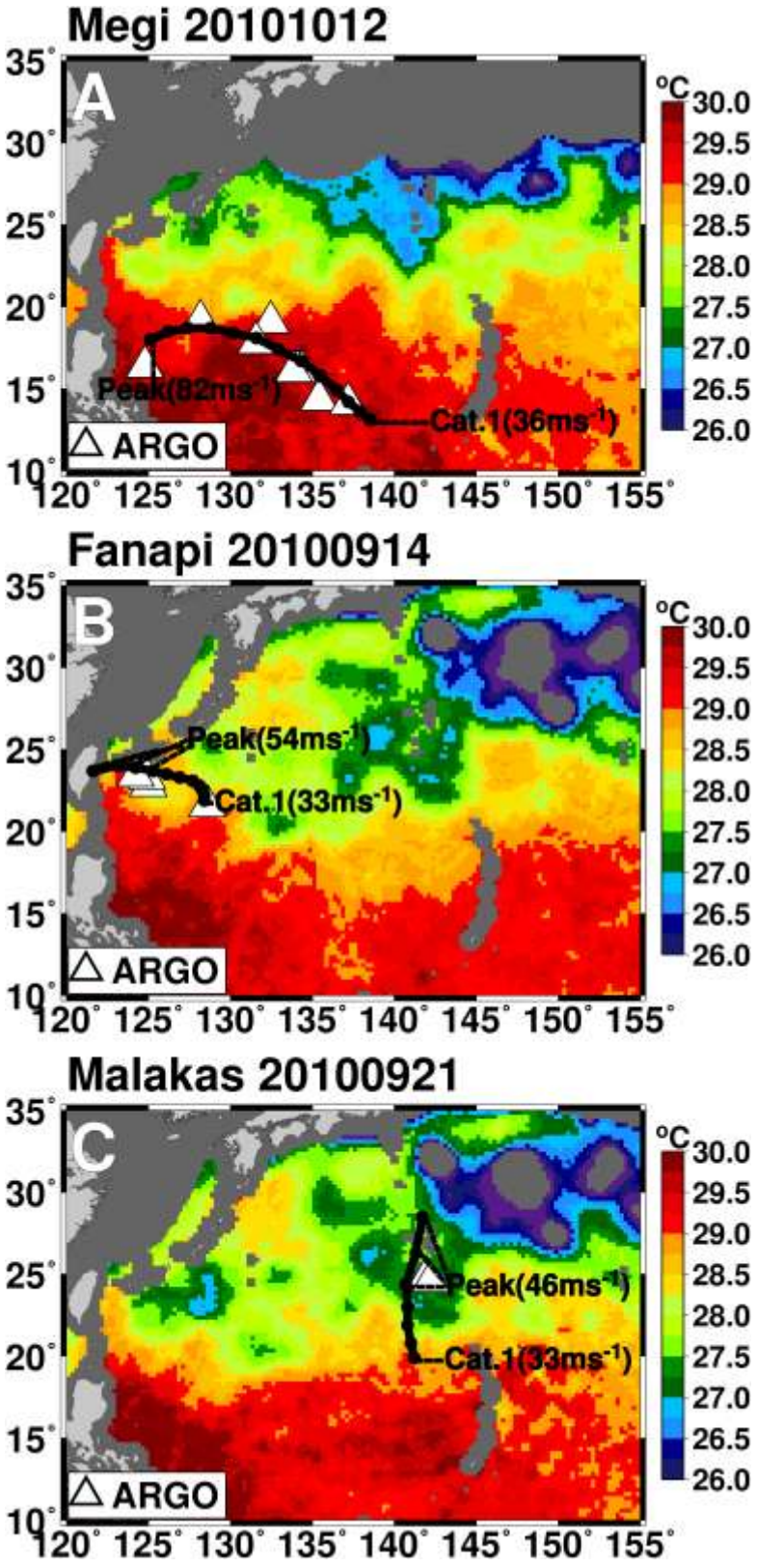

Fig. S4: As in S2, but for the corresponding pre-cyclone T80.

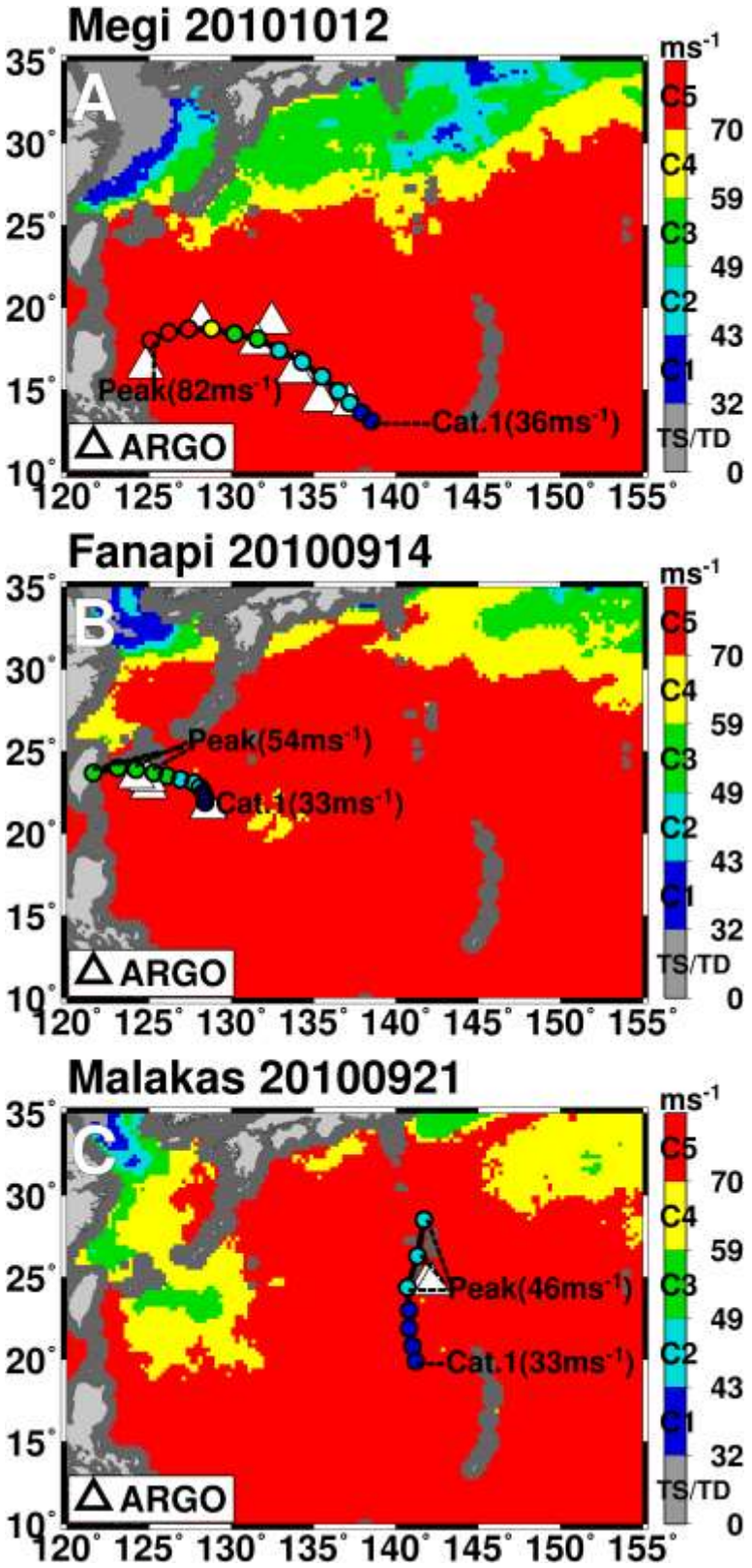

Fig. S5: As in S1, but for the pre-cyclone SST_PI calculated using input from Fig. S1, showing little distinction in ocean's realistic potential as category-5 intensity is predicted for most parts of the basin. It can be seen that the SST_PI is much higher than the observed maximum (peak) intensity of Fanapi (category-3) and Malakas (category-2).

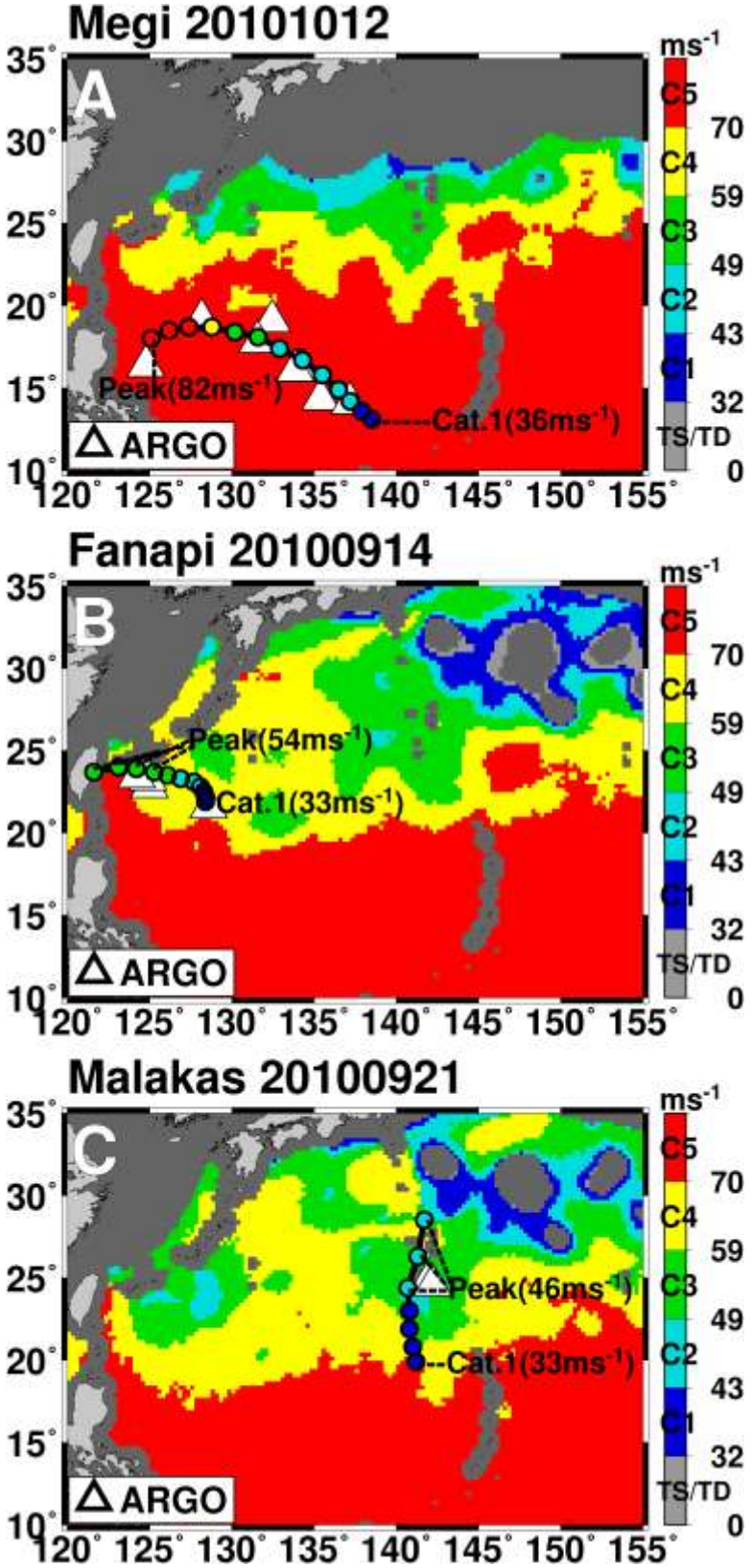

Fig. S6: As in S5, but for the pre-cyclone OC_PI_T80.

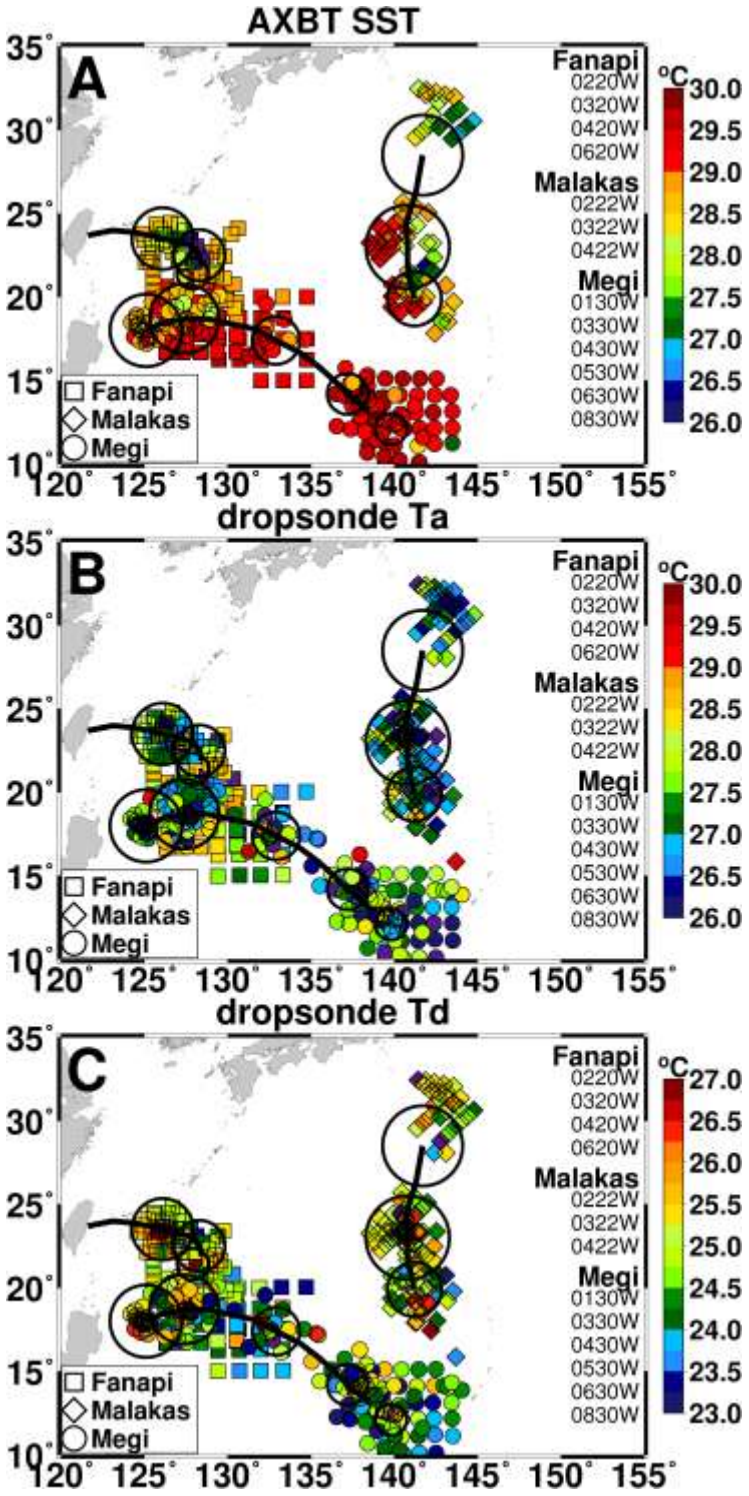

Fig. S7: (A) *In situ* during-intensification AXBT SST observations from the TC-penetrating flights of the ITOP campaign. The circles denote the 34 kt wind radius from the JTWC data base. **(B)** As in (A), but for the near co-incident and co-located ocean surface atmospheric temperature data from the dropwindsondes. **(C)** As in (B), but for the ocean surface atmospheric dew point temperature data.

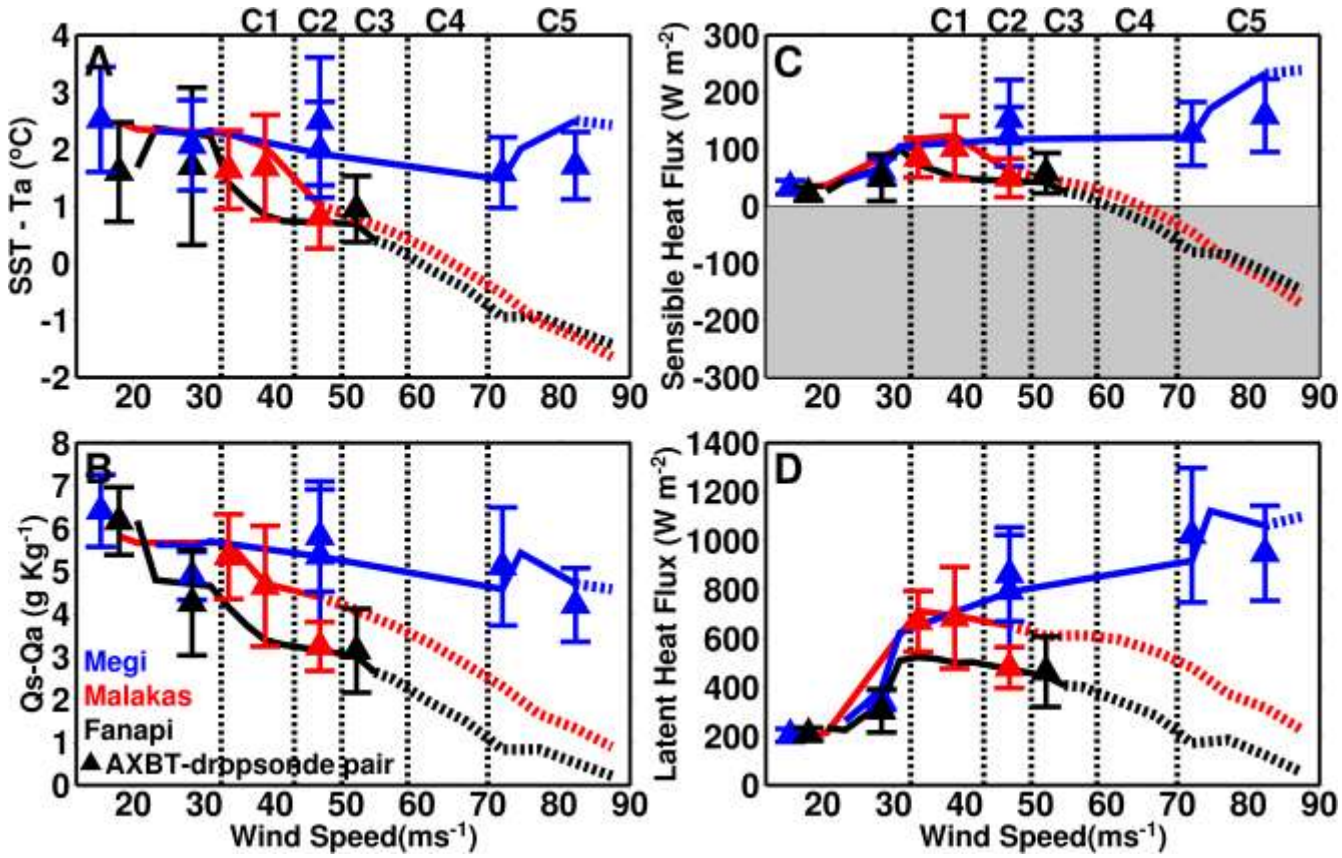

146

147

148 **Fig. S8: (A)** During-intensification air-sea temperature difference (points with error bars) based on the
149 difference between the AXBT and dropwindsonde observations. Solid and dash lines are difference
150 based on the simulated SST of the 3D ocean mixed layer simulations. (**B**) As in (A), but for the air-sea
151 moisture difference. (**C**) Sensible heat flux estimated based on input using (A) (see Sec. 4 in SOM). (**D**)
152 Latent heat flux estimated based on input using (B).

153

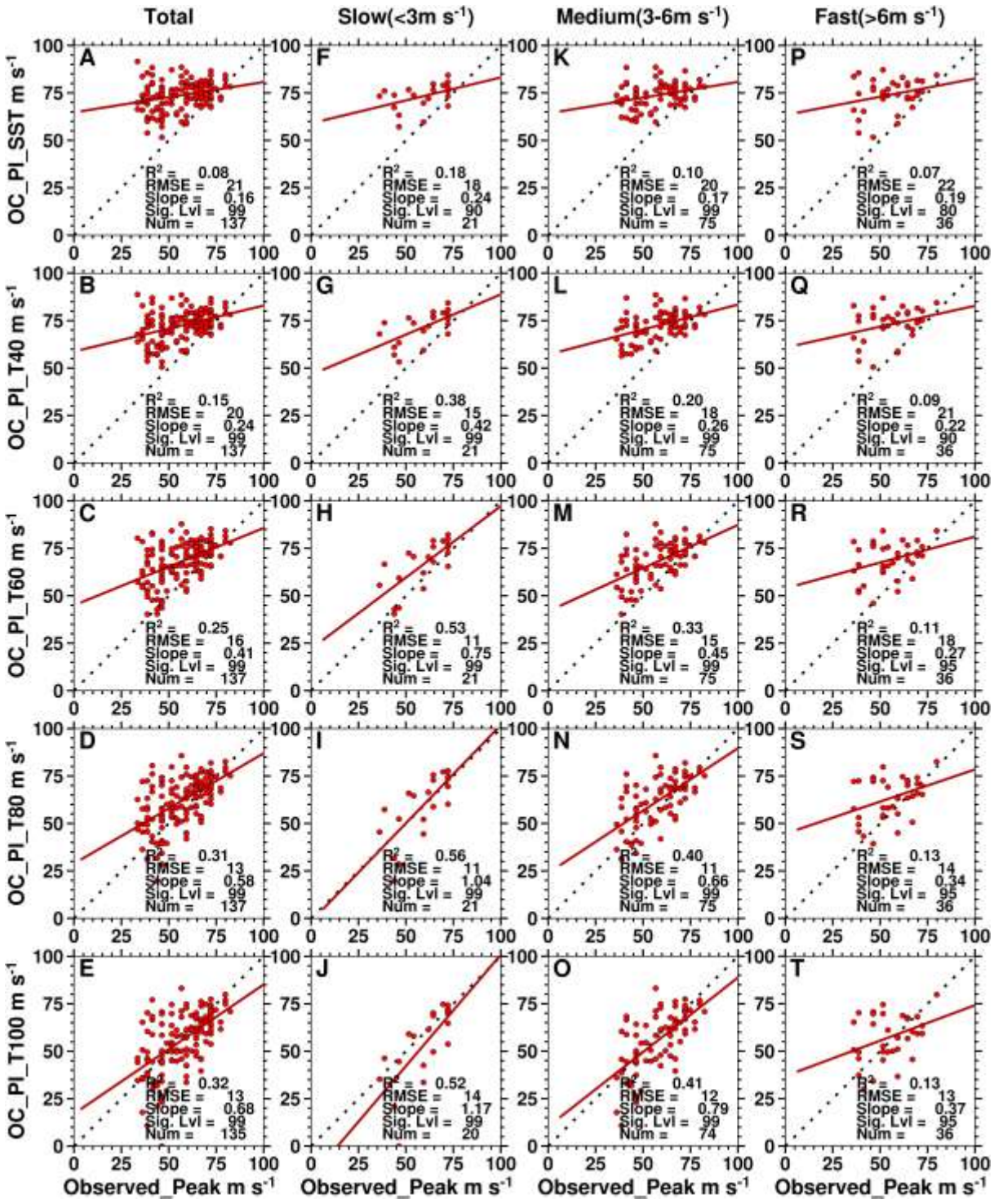

Fig. S9: (**A**) Predicted maximum intensity using SST_PI verses the observed maximum (peak) intensity for 14-years (1998-2011) of western North Pacific TCs (137 cases). The dashed-diagonal line is the best possible prediction (i.e. slope=1). **(B)-(E):** As in (A), but for OC_PI_T40 to OC_PI_T100. **(F)-(J):** As in (A) to (E), but for the subset of slow-moving TCs (translation speed: 0-3 ms^{-1}). **(K)-(O):** As in (F)-(J), but for the subset of medium-moving TCs (3-6 ms^{-1}). **(P)-(T):** As in (F)-(J), but for the subset of fast-moving TCs (6-9 ms^{-1}). The results for OC_PI_T20 is similar to SST_PI and are not shown.

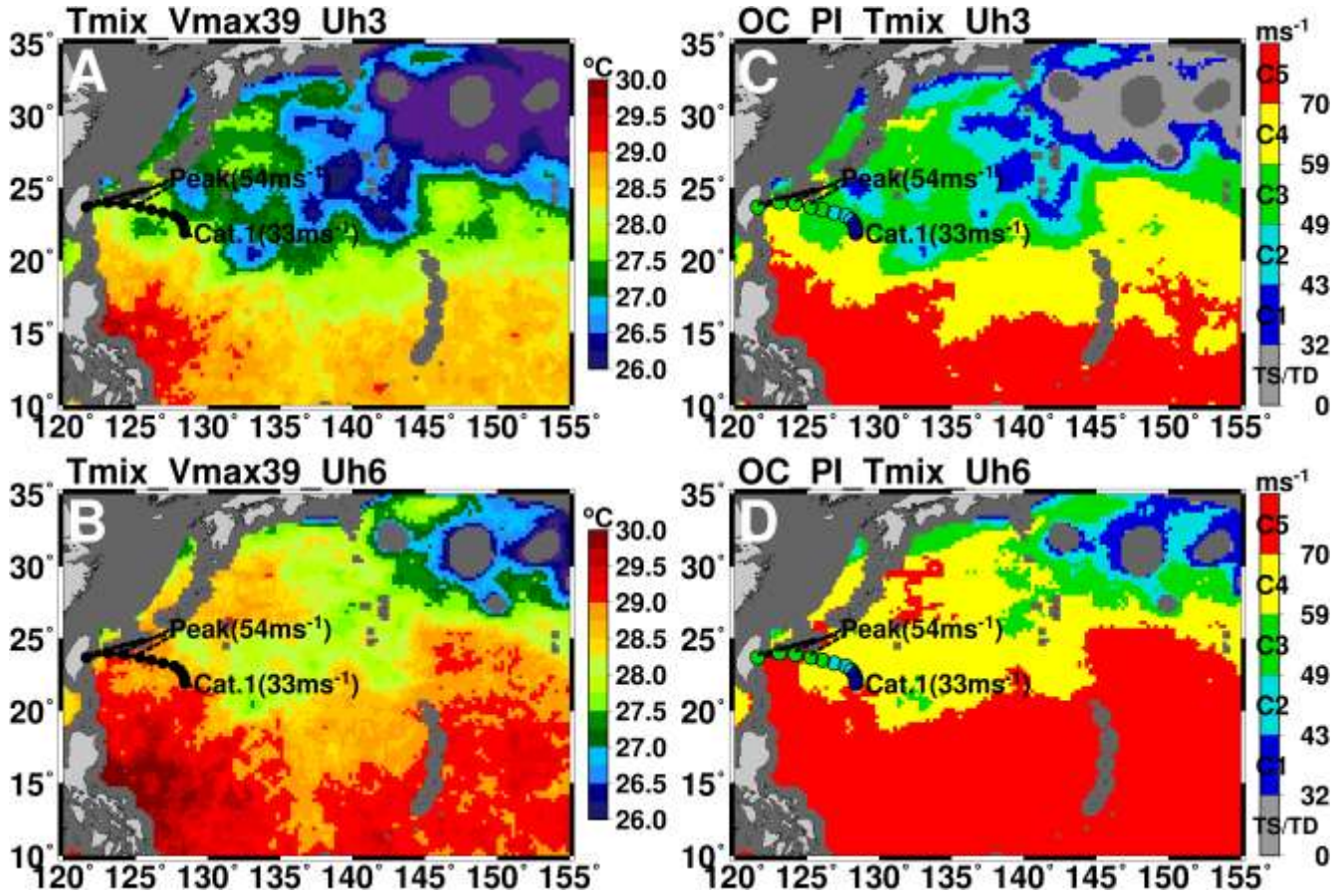

Fig. S10: As in S6, but for the case of Fanapi using $\overline{T}$ calculated based on (*19*) under two translation speeds (3 and 6 ms^{-1}). **(A)** and **(B)**: $\overline{T}$ calculated under 3 and 6 ms^{-1}. **(C)** and **(D):** as in (A) and (B), but for the corresponding OC_PI. It can be seen that as Fanapi was relatively-slow moving during intensification (average translation speed = 3.2 m s^{-1}), OC_PI based on 3 m s^{-1} was close to the observed peak, while OC_PI based on 6 m s^{-1} (less cooling) does not perform as well because of over-estimation.

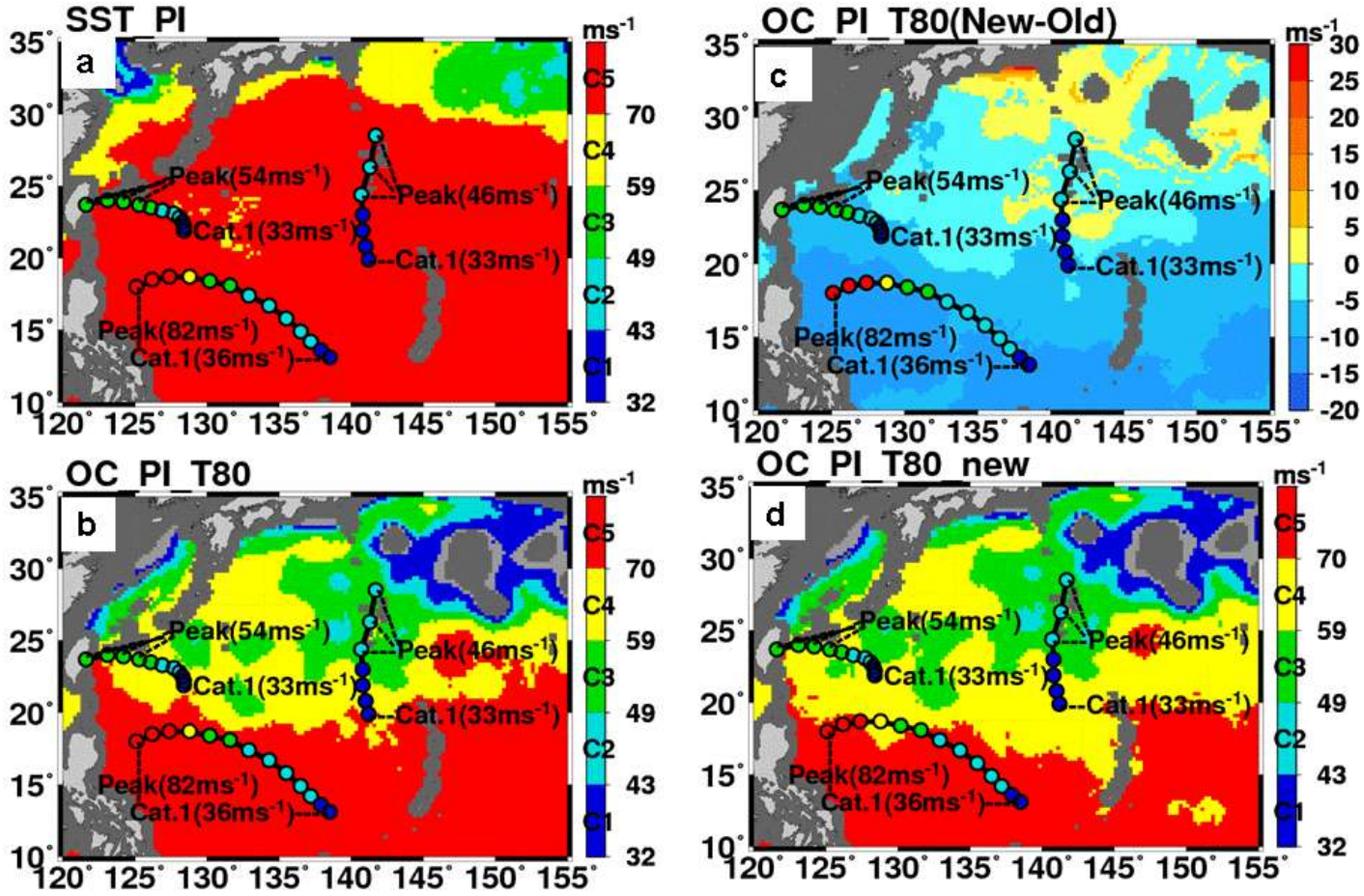

Fig. S11: (a) SST_PI as in Fig. 1A of the paper. (b) OC_PI as in paper Fig. 1D. (c) Difference between OC_PI and OC_PI_new. (d) OC_PI_new, as obtained through replacing the lowest level air temperature with $\overline{T}$.

Supplementary Table:

	No. of profiles	SST (° C)	D26 (m)	UOHC (Kj cm^{-2})	T80 (° C)
Megi	12	29.8±0.25	111±16	128±22	29.3±0.38
Fanapi	4	29.2±0.24	68±18	67±23	27.7±0.71
Malakas	2	29.7±0.20	44±2	51±7	26.3±0.40

Table S1: Pre-cyclone SST, D26, UOHC, and T80 from the Argo profiles (Fig. 2A) for the 3 ITOP cases.